Hindawi
International Journal of Antennas and Propagation
Volume 2023, Article ID 6227251, 12 pages
https://doi.org/10.1155/2023/6227251

Research Article

A Millimeter-Wave Antipodal Linearly Tapered Slot Antenna Array for 5G Wireless Communication

C. Ni,[1] W. W. Wang,[2] Y. C. Zheng,[1] J. Ding,[1] K. Cao,[1] and B. Liu[2]

[1]*State Grid Yangzhou Power Supply Company, Jiangsu 225000, Yangzhou, China*
[2]*College of Electronic and Information Engineering, Nanjing University of Aeronautics and Astronautics, Jiangsu 211100, Nanjing, China*

Correspondence should be addressed to B. Liu; doctice@hotmail.com

Received 13 March 2023; Revised 7 July 2023; Accepted 8 July 2023; Published 21 July 2023

Academic Editor: Claudio Gennarelli

This paper presents an antipodal linearly tapered slot antenna (ALTSA) array with the newly emerging substrate-integrated coaxial line (SICL) technology. Each element of the proposed array consists of two vertically stacked antipodal tapered slot antennas (TSA) with the inner conductor of a SICL as the shared fin. The vertical symmetry of this radiating element structure significantly suppresses the cross-polarization level. By employing a SICL-based power splitter with differential outputs, a two-element array with horizontal symmetry is formed. With the inner conductors of two parallel SICLs combined as the flaring metal shared by adjacent tapered slots, the main beam squint is effectively suppressed. Experimental results show an actual −10-dB impedance bandwidth (BW) of 24.5~34.4 GHz, and the realized gain range measured is 16.1~18.7 dBi. The cross-polarization levels are −39.4 dB/−40.7 dB at 30 GHz for the E-/H-planes. The measured results agree well with the simulated data which demonstrates the feasibility of the proposed SICL-based ALTSA scheme in the potential 5 G·millimeter-wave (mmWave) applications.

1. Introduction

Nowadays, the growing demands for high data rate communication and short-range detection have stimulated the applications of millimeter wave (mmWave) [1–3]. However, transmission in the mmWave band is susceptible to environmental factors such as raindrops and oxygen absorption [4, 5], which calls for high-gain and low-cross-polarization antenna designs. Tapered slot antenna (TSA), also known as the Vivaldi antenna, is one of the promising candidates [6–9] featuring broadband, low weight, low profile, ease of fabrication, and integration with microwave circuits [10]. Recently, the development of substrate-integration technologies has enabled using the substrate-integrated waveguide (SIW) technology as the feed of the antipodal TSAs [11–19]. Compared with conventional microstrip-based feed, the SIW-based feed achieves a broader bandwidth and can provide a phase reversal excitation for the antipodal TSA without using a balun. However, the performances of these SIW-based schemes are susceptible to substrate thickness, permittivity, and antenna geometry. Specifically, two issues need to be fixed. One is that the cross-polarization level of the antipodal TSA increases with the substrate thickness as it is vertically asymmetric. The other is that the dispersive characteristic of SIW restrains bandwidth enhancement and structural miniaturization. Lately, a substrate-integrated technology, termed substrate-integrated coaxial line (SICL), has been proposed. It is a two-wire nondispersive transmission line with ultra-slim size, which is suitable to meet the design requirement of wideband and miniaturization [20]. As shown in Figure 1, SICL comprises a conductive signal strip sandwiched between two grounded substrates and bounded bilaterally by two rows of metallic vias, which constrains the undesired parallel-plate mode. The nondispersive characteristic of SICL makes it competitive in designing broadband feeds [21] and compact antennas [22, 23].

In this paper, a balanced antipodal linearly taper slot antenna comprising two vertically stacked antipodal TSAs is

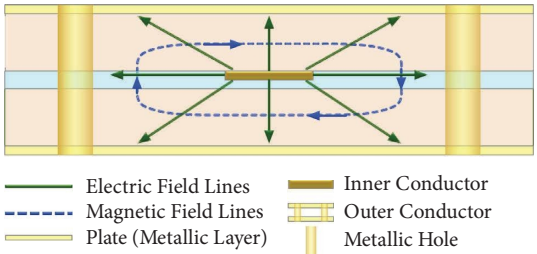

Figure 1: Cross-sectional view of a SICL (not to scale).

proposed. As shown in Figure 2, SICL is employed as the feed with its inner conductor as a shared fin of the two antipodal TSAs.

The vertical symmetry of the proposed structure significantly suppresses the vertical E-field and the cross-polarization level. Furthermore, a two-element antenna array is implemented with considerable gain and cross-polarization enhancement.

The remaining contents are organized as follows. Section 2 elaborates on the designs of both the radiating element and the array. Section 3 details the experimental verification. Section 4 concludes the whole work.

2. Antenna Design

The design procedure comprises two phases: design of the SICL-based TSA radiating element and design of the 1×2 array.

2.1. Design of the Radiating Element. ALTSA is known to have a high input impedance, which causes an impedance mismatch to the SICL feed, as the characteristic impedance of the SICL is relatively low. To solve this problem, we propose a SICL-based tapered slot element with which the inner strip of SICL protrudes and is expanded into the trapezoidal fin of the tapered slot. As depicted in Figure 3, the element consists of three plates and two dielectric substrates with an intermediate prepreg for bonding. The fin in the middle plate is ungrounded and antipodal to the top/bottom fins etched in the top/bottom plates. The top/middle/bottom fins gradually flare at a constant angle, making up the shunt up/low TSAs, and consequently lower the input impedance. Thus, the impedance matching between the ALTSA and the SICL can be realized without additional transition.

Conventional TSAs, such as SIW-based schemes, are realized by flaring the grounded plates on both sides of the substrate in the opposite direction with the electric field intensity vector ($\vec{E}$) inclined to the horizontal plane. As is illustrated in Figure 4(a), while the horizontal component of the electric field ($\vec{E}_{\parallel}$) contributes to the effective radiation, a vertical component ($\vec{E}_{\perp}$) due to the structural asymmetry cannot be eliminated and causes the unwanted cross-polarization.

Unlike the SIW-based scheme with all fins grounded, the proposed SICL-based scheme herein has a vertical symmetry as sketched in Figure 4(b). Since the top/bottom fins are grounded, the E-vector inside the triple-plate structure consists of two symmetric components, $\vec{E}_1$ and $\vec{E}_2$. With the thickness of the prepreg to be small enough (0.1 mm in this design), the difference between the magnitudes of $\vec{E}_{1\perp}$ and $\vec{E}_{2\perp}$ is subtle and can be neglected. So $\vec{E}_{2\perp}$ can be considered as the negative vector of $\vec{E}_{1\perp}$, and $\vec{E}_{1\perp} + \vec{E}_{2\perp} = 0$. As a consequence, the source that causes cross-polarization is eliminated.

Once the impedance matching condition is satisfied, the dimensions of the tapered slot can be determined with the well-studied method [24–33]: Firstly, the length of the tapered slot line (l_{ts}) is determined. A typical value is $3\lambda_0 \sim 8\lambda_0$, where λ_0 is the free-space wavelength. Secondly, the width of the open end of the tapered slot line (w_{ts}) is determined, which is usually more than $0.5\lambda_0$. Thirdly, since the performance of the ALTSA is quite sensitive to the relative permittivity (ε_r), the substrate thickness (t_{sub}) can be determined in the range of $0.005\lambda_0/(\sqrt{\varepsilon_r} - 1) \le t_{sub} \le 0.03\lambda_0/(\sqrt{\varepsilon_r} - 1)$. Given the designed center frequency at 30 GHz, we can have $l_{ts} = 5\lambda_0 = 50$ mm and $w_{ts} = 1.1\lambda_0 = 11$ mm, respectively. The corrugation structures are etched in the outer edges of the fins to alter the phases of edge currents so that both the gain drop and the near-field radiation caused by the undesired surface currents at the outer edges can be suppressed [27, 28]. In the meanwhile, for corrugation lengths (rcl) under $0.14\lambda_0$, small changes will cause an obvious impact on the E-plane beamwidth, and the H-plane beamwidth variations in this region are less severe.

The simulated performance of the proposed TSA element is demonstrated in Figure 5. As is seen in the figure, the −10-dB impedance bandwidth is 25.3~32.9 GHz, and the in-band gain is flat and has a peak value of 17.1 dBi. The E- and H-plane patterns at 30 GHz are illustrated in Figure 5(b), which shows a gain of 16.98 dBi and a cross-polarization level of −37.2 dB. Although the radiating element has effectively suppressed the cross-polarization, the asymmetry of its structure causes a beam squint. The issue can be fixed by using asymmetric substrate cutouts and dual-scale slotted edges. In our work, the beam squint is eliminated by employing an 1×2 array with a differential feed, as is discussed in the following section.

2.2. Design of the Array. To feed a TSA array, a SICL-based equal-split power divider is designed first. It consists of a microstrip-to-SICL transition and a pair of differential outputs. As shown in Figure 6, two trapezoid slots of length asl_0 and asl_1 with widths asw_0, asw_1, and asw_2 are, respectively, etched in the top plate. These two slots are used to mitigate the abrupt E-field variation aroused by the junction of transition. The microstrip line is connected to the SICL inner conductor with a tapered transition for impedance matching. The metallic vias on both sides of the microstrip line prevent the excitation of spurious parallel plate waveguide mode between the conducting strip and the bottom plate. Meanwhile, complementary split-ring resonators (CSRRs) are etched in the top and bottom plates on both sides of the SICL to suppress the surface currents.

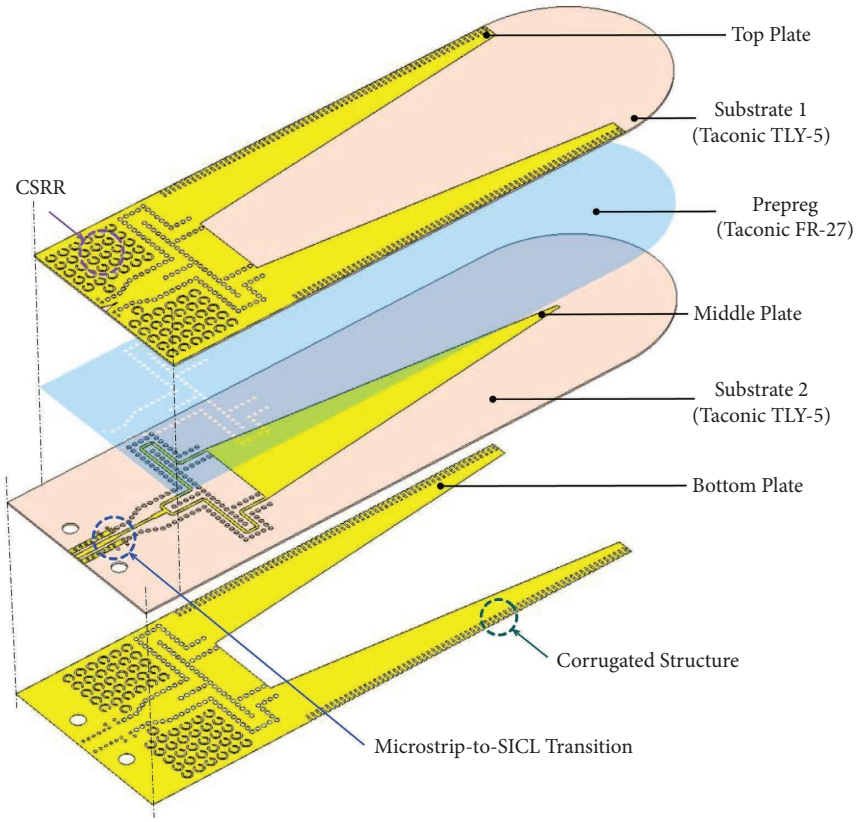

Figure 2: Geometry of the proposed BALTSA array.

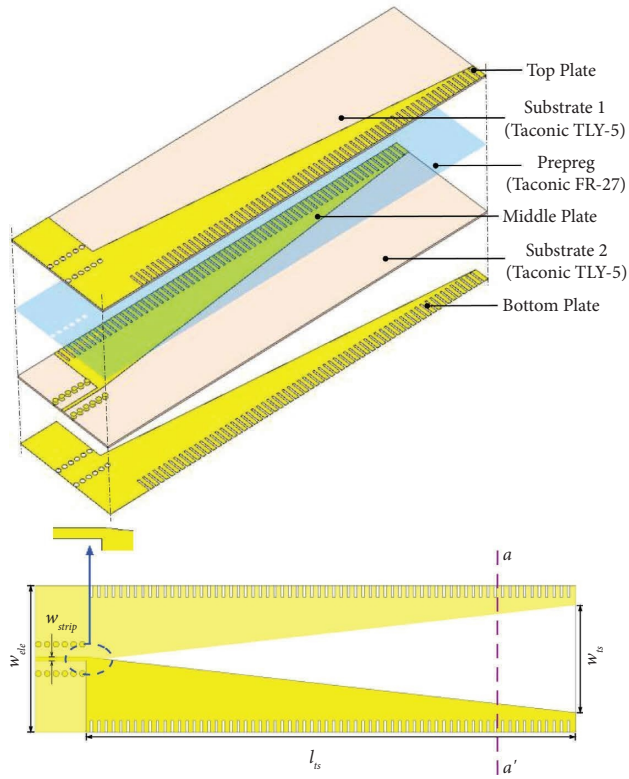

Figure 3: Geometry of the proposed SICL-based ALTSA element. The dimensions are (in mm) $w_{ele} = 15.0$, $w_{strip} = 0.4$, $l_{ts} = 50.0$, $w_{ts} = 11.0$.

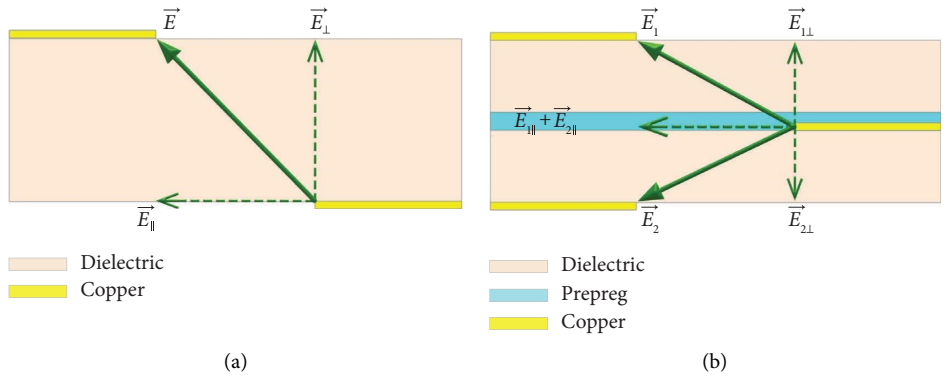

Figure 4: Electric field intensities in the cross-sections of the TSA elements. (a) The conventional SIW-based scheme. (b) The proposed SICL-based scheme (at *aa*') corrugation.

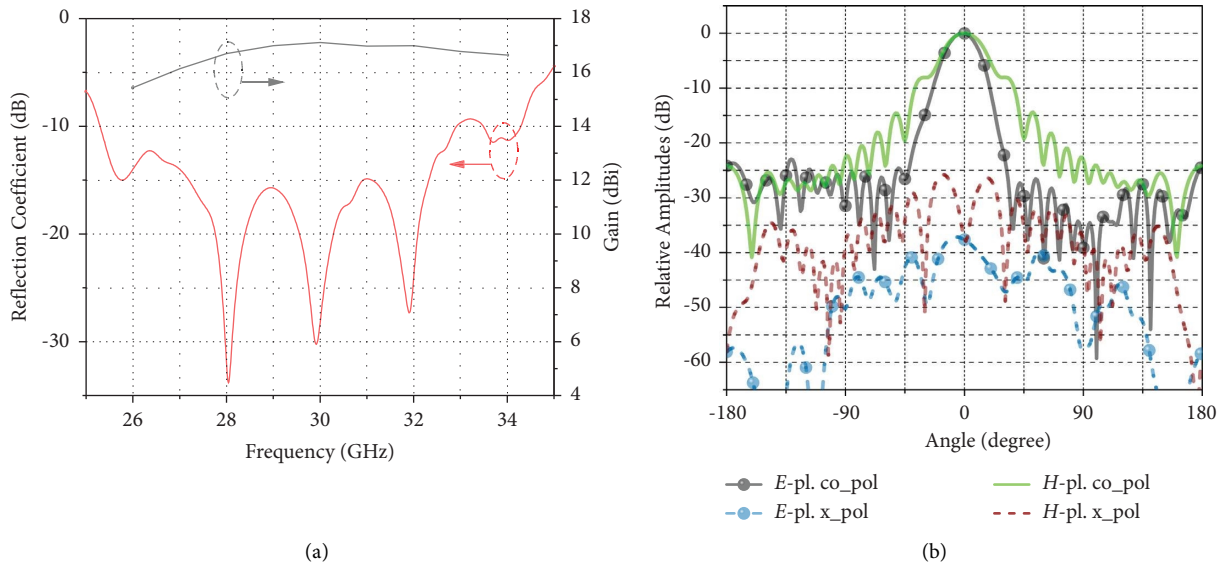

Figure 5: Simulated performances of the TSA element. (a) Gain and reflection coefficient performance. (b) Radiation patterns at 30 GHz.

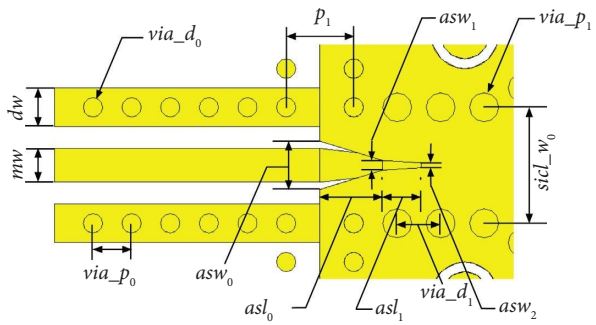

Figure 6: Geometry of the microstrip-to-SICL transition. The dimensions are (in mm) $asl_0 = 1.3$, $asl_1 = 0.8$, $asw_0 = 1.0$, $asw_1 = 0.2$, $asw_2 = 0.1$, $dw = 0.8$, $mw = 0.7$, $p_1 = 1.4$, $sicl\_w_0 = 2.4$, $via\_d_0 = 0.4$, $via\_d_1 = 0.6$, $via\_p_0 = 0.8$, $via\_p_1 = 0.9$.

With the phase-reversal excitation and the TSA element designed above, a 1×2 array is formed as illustrated in Figure 7 with the geometrical specifications. The trapezoidal metal sheets connected to the inner and outer conductors of the SICL build a balanced structure of ALTSA. The corresponding E-field distribution is shown in Figure 8(a). A semielliptical-shaped dielectric guiding structure is added as a dielectric lens in front of the array to narrow the beamwidth in *E*-plane, enhancing the gain as discussed in [33]. Meanwhile, according to the E-field plotted in Figure 8(b),

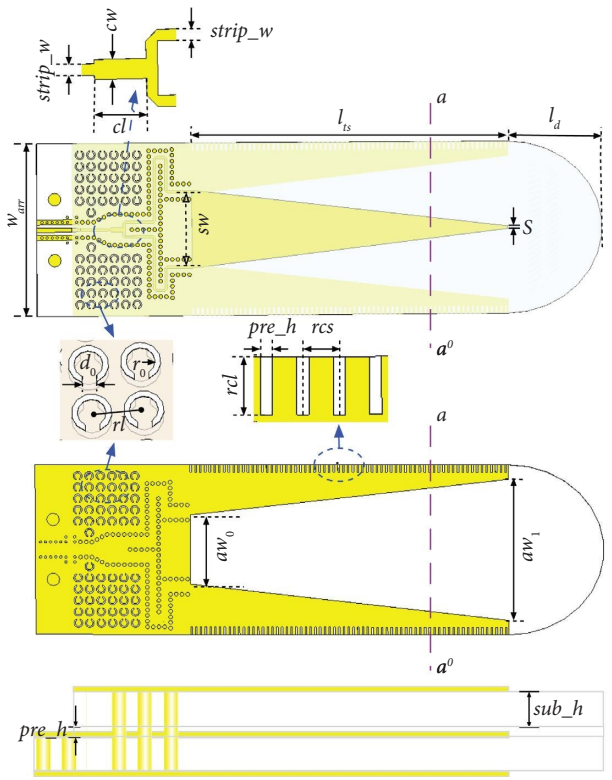

FIGURE 7: Geometry of the proposed 1×2 array. The dimensions are (in mm) $aw_0 = 11.0$, $aw_1 = 22.4$, $c_1 = 1.8$, $cw = 0.7$, $d_0 = 0.5$, $r_0 = 0.7$, $rcl = 1.2$, $rcs = 0.75$, $rcw = 0.25$, $rl = 1.8$, $s = 0.4$, $strip\_w = 0.4$, $sw = 11.4$, $w_{arr} = 27.0$, $l_{ts} = 50.0$, $l_d = 15.0$.

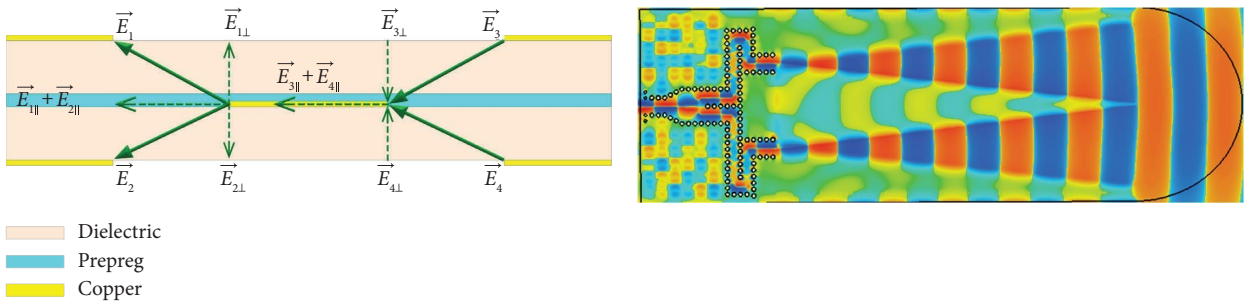

(a) (b)

FIGURE 8: (E)-field distribution in the array. (a) E-field (cross-sectional view at aa'). (b) E-field (top view).

we can safely assume that the proposed array is equivalent to an 1×2 array. The simulated beam squints about the element and array are shown in Figure 9, where we can find that the proposed array fed by odd-mode excitation has a lower beam squint than that of the element designed above.

3. Experimental Verification

To verify the feasibility of the proposed SICL-based ALTSA array, we have fabricated it using the standard PCB process, as presented in Figure 10. The prototype consists of two dielectric layers (Taconic TLY-5, $\varepsilon_r = 2.2$, $\tan\delta = 0.0009$, 0.254 mm in thickness) bonded by a prepreg (Taconic $fastRise^{TM}$ FR-27, $\varepsilon_r = 2.77$, $\tan\delta = 0.0017$, 0.1 mm in thickness), and two metallic layers (35 μm in thickness). The overall size is 89.4 mm × 27 mm × 0.608 mm. A 2.40-mm end launch connector [34] is used in the measurement.

The reflection coefficient is measured over the frequency range of 24~35 GHz by using a vector network analyzer (R&S ZVA50). As illustrated in Figure 11, the −10-dB impedance bandwidth is 9.9 GHz (24.5~34.4 GHz, 33% @30 GHz). Since TSA usually includes none resonant structures, manufacturing tolerances do not strongly influence its operating frequency or radiation. The measured center frequency is 29.45 GHz, which is 550 MHz lower than the designed value of 30 GHz.

The radiation performance is measured by using the far-field method in an anechoic chamber (see Figure 12). The gain is measured from 24~33 GHz, as shown in Figure 13. A measured peak gain of 18.77 dBi is observed at 33 GHz (the insertion loss

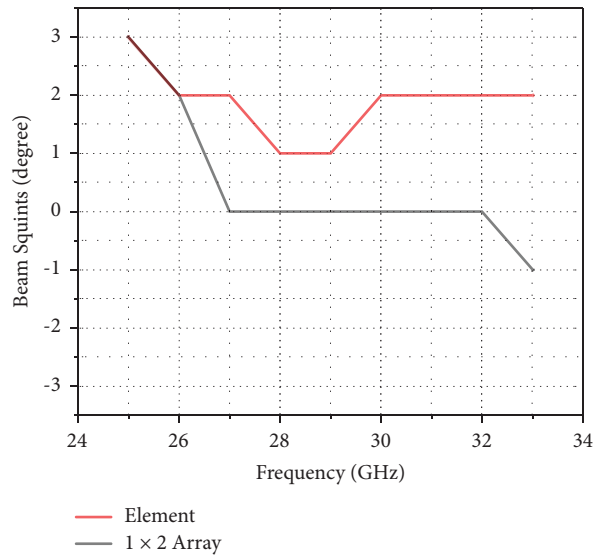

Figure 9: Comparison of the beam squints (simulated values).

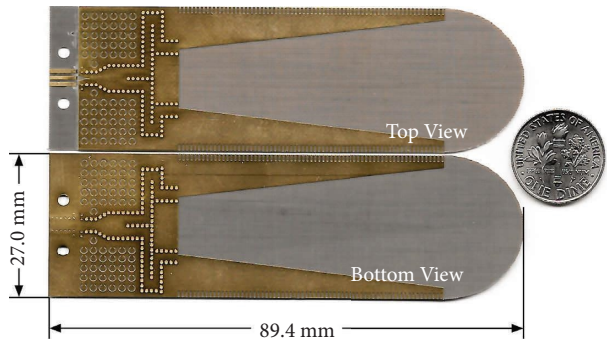

Figure 10: Photograph of the proposed array.

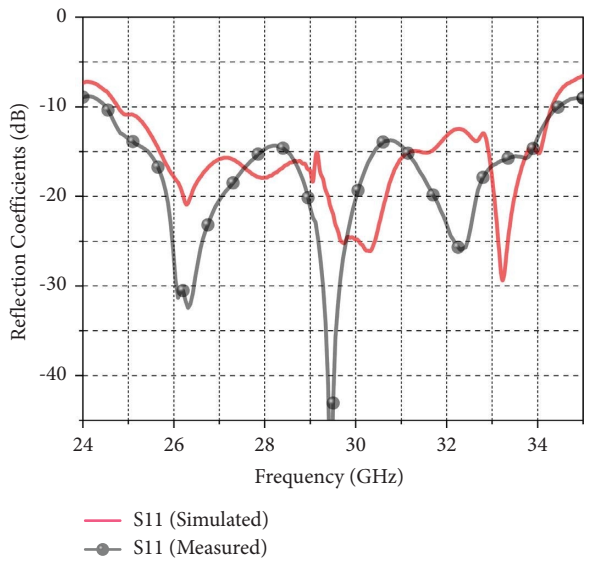

Figure 11: The simulated and measured reflection coefficients.

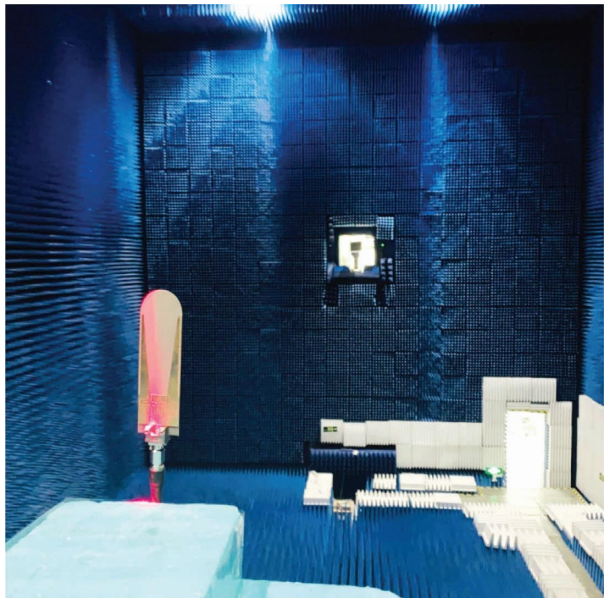

Figure 12: Far-field test environment.

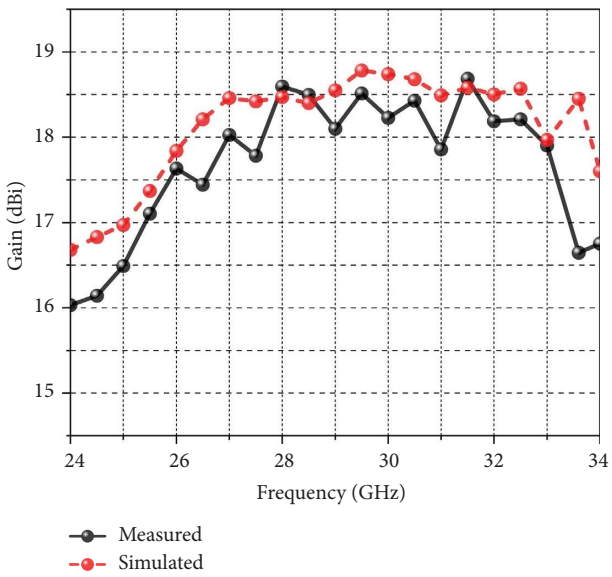

Figure 13: The simulated and measured gain performance.

of the end launch connector, which is about 0.84 dB at 30 GHz, has been excluded), while the maximum gain in simulation is 18.81 dBi. The corresponding details are illustrated in Figure 13. In the meanwhile, the simulated antenna efficiency in the entire operating frequency band is greater than 75%. The cross-polarization performance versus frequency is plotted in Figure 14. According to the configuration of the array, both the E-plane and the H-plane have the same cross-polarizations, and the simulated values are −33.2 dB @ 27 GHz, −45.0 dB @ 30 GHz, and −24.0 dB @ 33 GHz, respectively. The measured cross-polarizations at 27 GHz, 30 GHz, and 33 GHz are−34.7 dB, −39.4 dB, and −24.7 dB for the E-plane and −31.6 dB, −40.7 dB, and −26.1 dB for the H-plane.

There is a small difference between the two principal planes' values. This is because the main-lobe direction of the antenna does not point exactly toward the direction with zero degree angle due to the alignment error when the antenna was mounted on the turntable. The cross-polarization levels increase slightly as the operating frequency deviates from the center frequency of 30 GHz. This is caused by the limited bandwidth of the SICL balun. Figure 15 shows the E-plane and the H-plane radiation patterns of the proposed array at 27 GHz, 30 GHz, and 33 GHz. It can be found that the E-plane beamwidth is narrower than that of the H-plane, which is caused by the horizontal arrangement of the two radiating elements in the array.

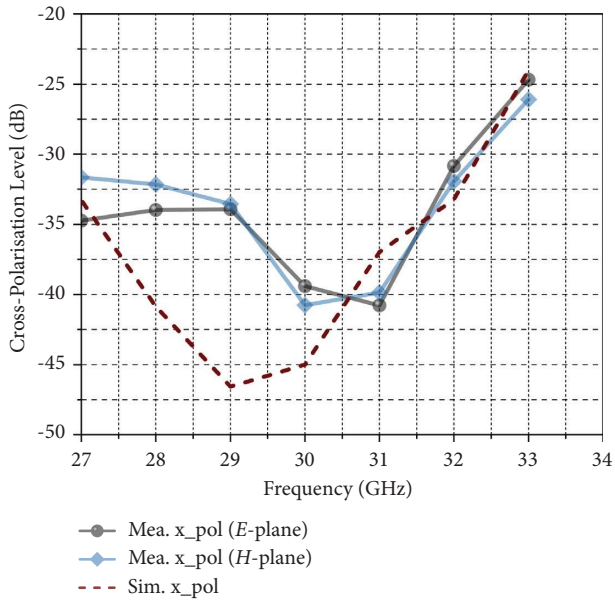

Figure 14: The simulated and measured cross-polarization.

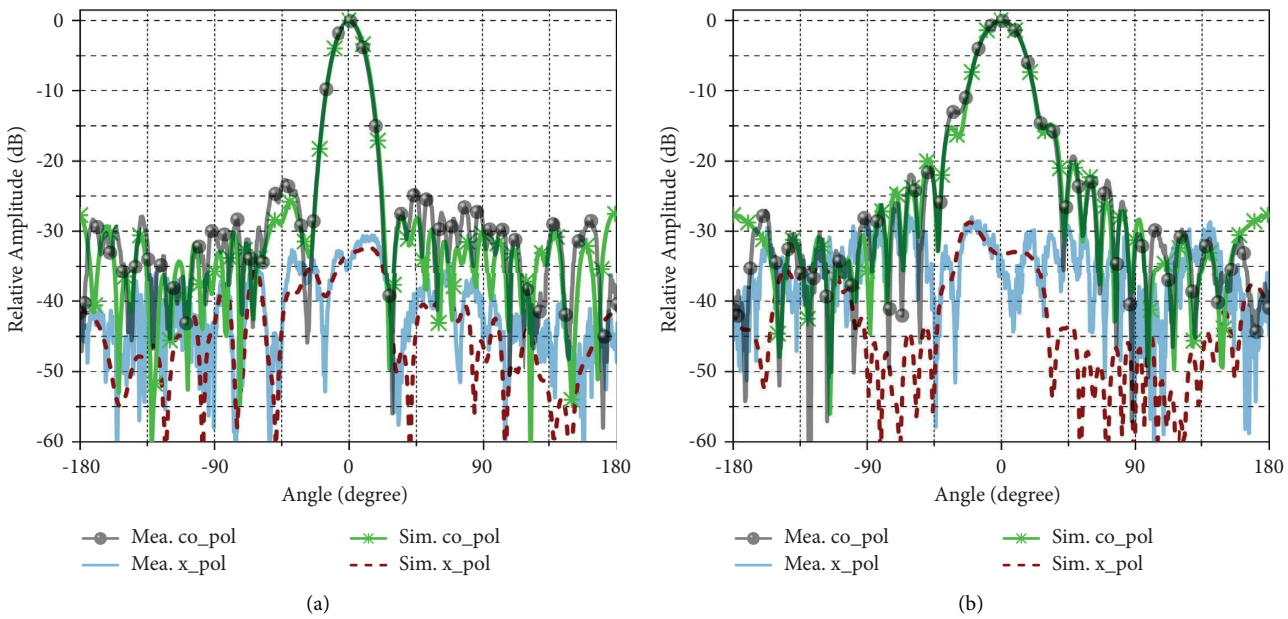

Figure 15: Continued.

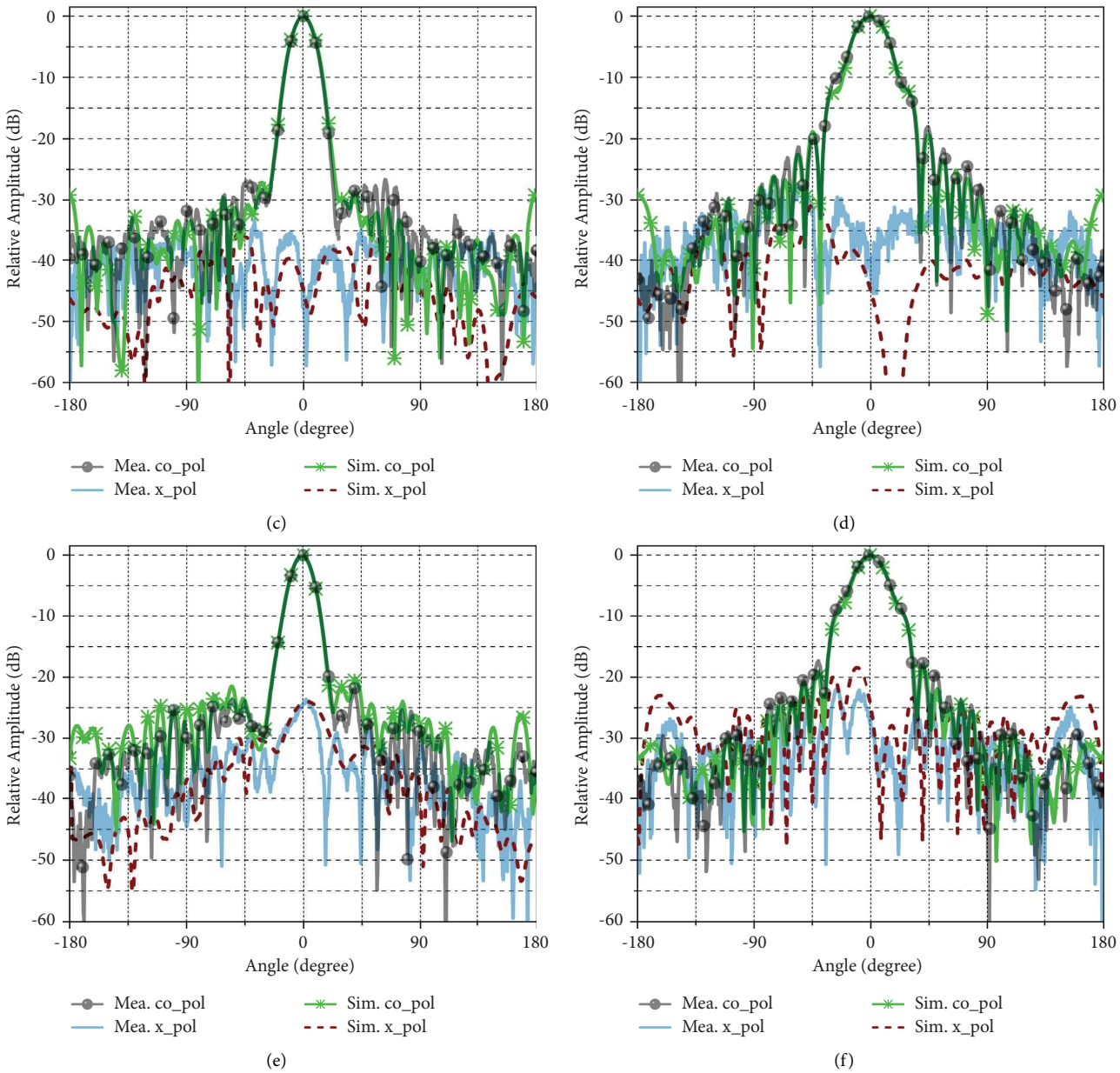

FIGURE 15: The simulated and measured radiation patterns. (a) E-plane at 27 GHz. (b) H-plane at 27 GHz. (c) E-plane at 30 GHz. (d) H-plane at 30 GHz. (e) E-plane at 33 GHz. (f) H-plane at 33 GHz.

Table 1: Comparison of this work with other reported works.

Item	This work	[8]	[13]	[18]	[19]	[30]	[31]
Publication year	N/A	2020	2020	2013	2021	2018	2017
Antenna type	ALTSA	AVA	AVA	ALTSA	ALTSA	BAVA	AVA
Topology type	SICL	Microstrip	DRSIW	SIW	SAFSIW	Stripline	Microstrip
Substrate type	2-Layer	1-Layer	3-Layer	1-Layer	3-Layer	2-Layer	1-Layer
Permittivity (ϵ_r)	2.2	2.2	2.2	2.94	2.94 2.2	2.2	2.65
Thickness (mm)	0.608	0.787	2.361	0.508	1.524	0.508	1
Centre freq. (GHz)	30	26.5	25	26	33	25	8.9
Fractional bandwidth	33%	15.34%	113.73%	38.4%	40.9%	120%	137%
Gain (dBi)	16.68~18.77	9.41~11.44	2.15~5.75	10~18	11.65~14.35	9.6~15	0~15
E-plane X-pol (dB)	−34.7@27 GHz −39.4@30 GHz −24.7@33 GHz	−12@26 GHz −10@28 GHz	−16@15 GHz −8@25 GHz −10@33 GHz	−17.0@24 GHz −22.0@28 GHz −10.8@31 GHz	−17.5@29 GHz −22.0@33 GHz −22.5@37 GHz	−32@10 GHz −21@30 GHz −18@40 GHz	−35.0@2.8 GHz −29.3@10 GHz −24.8@15 GHz
H-plane X-pol (dB)	−31.6@27 GHz −40.7@30 GHz −26.1@33 GHz	−12@26 GHz −10@28 GHz	−18@15 GHz −8@25 GHz −8@33 GHz	−19.5@24 GHz −22.0@28 GHz −10.8@31 GHz	N/A	N/A	−40.0@2.8 GHz −29.3@10 GHz −24.8@15 GHz
Size ($\lambda 0 \lozenge \lambda 0$)	8.94◊2.7 (1◊2 array)	6.18◊2.97 (1◊8 array)	1.91◊0.83	(≥7.78)◊0.88	~7.2◊~2.3	6.66◊2	2.08◊1.48

A comprehensive performance comparison between the proposed antenna and other related antennas in the open literature is listed in Table 1, indicating that the proposed ALTSA design does have an apparent enhancement in cross-polarization performance.

4. Conclusions

This paper presents a balanced ALTSA fed by using the SICL technology, which provides a method to get a high gain with lower cross-polarization. The proposed ALTSA has a measured −10-dB impedance bandwidth of 33% centered at 30 GHz with a peak gain of 18.77 dBi observed in the measurement. The good agreement between the simulated and measured results demonstrates the feasibility of the proposed scheme with features of high gain and low cross-polarization, making it a possible candidate for antennas in millimeter-wave wireless communication.

Data Availability

The simulated and measured data of the proposed antenna used to support the findings of this study are available from the corresponding author upon request.

Conflicts of Interest

The authors declare that they have no conflicts of interest.

Acknowledgments

This work was supported by the National Natural Science Foundation of China under Grant 62171221.

References

[1] L. Mohamed, Z. Briqech, and A. Ssebak, "High-gain dielectric-loaded antipodal Femi tapered slot antenna for MM-wave applications," *Proc. ANTEM*, pp. 1-2, 2016.

[2] D. L. Brown and E. Rammos, *Communication Satellite Requirements for the Year 2000 and beyond*, IEE Colloquium on Satellite Antenna Technology in the 21st Century, London, UK, Jul. 1991.

[3] C. A. Balanis, *Modern Antenna Handbook*, John Wiley & Sons, Hoboken, NJ, USA, 2011.

[4] T. S. Rappaport, R. W. Heath, and R. C. Daniels, *Millimeter Wave Wireless Communications*, Prentice Hall, Hoboken, NJ, USA, 2015.

[5] P. F. M. Smulders, "Impact of Regulations on Feasible Distance between 60 GHz Devices," in *Proceedings of the Fourth European Conference on Antennas and Propagation*, Barcelona, Spain, July 2010.

[6] S. Prasad and S. Mahapatra, "A new MIC slot-line aerial," *IEEE Transactions on Antennas and Propagation*, vol. 31, no. 3, pp. 525–527, 1983.

[7] P. J. Gibson, "The Vivaldi Aerial," in *Proceedings of the 1979 9th European Microwave Conference*, pp. 101–105, Brighton, UK, September 1979.

[8] S. Zhu, H. Liu, P. Wen, Z. Chen, and H. Xu, "Vivaldi antenna array using defected ground structure for edge effect restraint and back radiation suppression," *IEEE Antennas and Wireless Propagation Letters*, vol. 19, no. 1, pp. 84–88, 2020.

[9] Z. N. Chen, T. Djerafi, and A. Doghri, "Substrate integrated waveguide antennas," in *Handbook of Antenna Technologies*, W. Ke, Ed., pp. 1616–1628, Springer Press, Singapore, 1 edition, 2016.

[10] K. S. Yngvesson, T. L. Korzeniowski, Y. S. Kim, E. Kollberg, and J. Johansson, "The tapered slot antenna-a new integrated element for millimeter-wave applications," *IEEE Transactions on Microwave Theory and Techniques*, vol. 37, no. 2, pp. 365–374, 1989.

[11] Z. C. Hao, W. Hong, and J. Chen, "A novel feeding technique for antipodal linearly tapered slot antenna array," *Proc. MTTs.*, pp. 1641–1643, 2005.

[12] X. Cheng, Y. Yao, J. Yu, and X. Chen, "Circularly polarized substrate-integrated waveguide tapered slot antenna for millimeter-wave applications," *IEEE Antennas and Wireless Propagation Letters*, vol. 16, pp. 2358–2361, 2017.

[13] J. Y. Deng, R. Cao, D. Sun, Y. Zhang, and L. X. Guo, "Bandwidth enhancement of an antipodal Vivaldi antenna facilitated by double-ridged substrate-integrated waveguide," *IEEE Transactions on Antennas and Propagation*, vol. 68, no. 12, pp. 8192–8196, 2020.

[14] T. Djerafi and K. Wu, "Corrugated substrate integrated waveguide (SIW) antipodal linearly tapered slot antenna array fed by quasi-triangular power divider," *PIER C*, vol. 26, pp. 139–151, 2012.

[15] P. Shrivastava and R. R. Thipparaju, "60 GHz radio link characteristic studies in hallway environment using antipodal linear tapered slot antenna," *IET Microwaves, Antennas & Propagation*, vol. 9, no. 15, pp. 1793–1802, 2015.

[16] T. R. Rao, C. Sarath, N. Tiwari et al., "Design of SIW fed antipodal linearly tapered slot antenna array with hat-shaped dielectric loading for 60 GHz wireless communications," *Proc. IAW.*, pp. 67–70, 2016.

[17] J. Guo, T. Djerafi, and K. Wu, "Balanced corrugated antipodal linear tapered slot antenna with integrated feeding for cross-polarisation suppression," *Proc. ANTEM.*, pp. 1–4, 2018.

[18] F. Taringou, D. dousset, J. Bornemann, and K. Wu, "Broadband CPW feed for millimeter-wave SIW-based antipodal linearly tapered slot antennas," *IEEE Transactions on Antennas and Propagation*, vol. 61, no. 4, pp. 1756–1762, 2013.

[19] N. H. Nguyen, A. Ghiotto, A. Vilcot, T. P. Vuong, and K. Wu, "Multilayer slab AFSIW antipodal linearly tapered slot antenna with cross-polarization reduction," *IEEE Antennas and Wireless Propagation Letters*, vol. 20, no. 5, pp. 763–767, 2021.

[20] F. Gatti, M. Bozzi, and L. Perregrini, "A novel substrate integrated coaxial line (SICL) for wide-band application," *Proc. EuMC.*, pp. 1614–1617, 2006.

[21] T. Y. Yang, W. Hong, and Y. Zhang, "An SICL-excited wideband circularly polarized cavity-backed patch antenna for IEEE 802.11aj (45 GHz) applications," *IEEE Antennas and Wireless Propagation Letters*, vol. 15, pp. 1265–1268, 2016.

[22] K. Xing, B. Liu, Z. Guo, X. Wei, R. Zhao, and Y. Ma, "Backlobe and sidelobe suppression of a Q-band patch antenna array by using substrate integrated coaxial line feeding technique," *IEEE Antennas and Wireless Propagation Letters*, vol. 16, pp. 3043–3046, 2017.

[23] L. Bing, X. Ke, W. Lei et al., "A novel slot array antenna with a substrate-integrated coaxial line technique," *IEEE Antennas and Wireless Propagation Letters*, vol. 16, pp. 1743–1746, 2017.

[24] J. Zucker, H. Jasik, *Surface- and Leaky-Wave Antennas," Antenna Engineering Handbook*, McGraw-Hill, Newyork, NY, USA, 1961.

[25] D. Schaubert, E. Kollberg, T. Korzeniowski, T. Thungren, J. Johansson, and K. Yngvesson, "Endfire tapered slot

antennas on dielectric substrates," *IEEE Transactions on Antennas and Propagation*, vol. 33, no. 12, pp. 1392–1400, 1985.

[26] T. J. Ellis and G. M. Rebeiz, "MM-wave tapered slot antennas on micromachined photonic bandgap dielectrics," *Proc. IEEE MTT-S Int. Microw. Symp. Dig.*, pp. 1157–1160, 1996.

[27] P. Shrivastava, D. Chandra, and N. Tiwari, "Investigations on corrugation issues in SIW based antipodal linear tapered slot antenna for wireless networks at 60 GHz," *Appl. Comput. Electrom.*,vol. 28, no. 10, pp. 960–967, 2013.

[28] T. R. Rao, P. Shrivastava, and N. Tiwari, "Investigations of corrugation issues in SIW based antipodal linear tapered slot antenna at 60 GHz," *Proc. EuCAP*, pp. 2104–2107, 2013.

[29] J. Langley, P. Hall, and P. Newham, "Novel ultrawide-bandwidth Vivaldi antenna with low cross polarisation," *Electronics Letters*, vol. 29, no. 23, pp. 2004-2005, 1993.

[30] N. N. Wang, M. Fang, H. T. Chou, J. R. Qi, and L. Y. Xiao, "Balanced antipodal vivaldi antenna with asymmetric substrate cutout and dual-scale slotted edges for ultra-wideband operation at millimeter-wave frequencies," *IEEE Transactions on Antennas and Propagation*, vol. 66, no. 7, pp. 3724–3729, 2018.

[31] Y. Wang and Z. Yu, "A novel symmetric double-slot structure for antipodal vivaldi antenna to lower cross-polarization level," *IEEE Transactions on Antennas and Propagation*, vol. 65, no. 10, pp. 5599–5604, 2017.

[32] S. Kirshna and S. Mukherjee, "Design of wideband microstrip to SICL transition for millimeter-wave applications," *IEEE Access*, vol. 8, pp. 4250–4254, 2019.

[33] N. Ghassemi and K. Wu, "Planar high-gain dielectric-loaded antipodal linearly tapered slot antenna for E- and W-Band gigabyte point-to-point wireless services," *IEEE Transactions on Antennas and Propagation*, vol. 61, no. 4, pp. 1747–1755, 2013.

[34] Datasheet of End Launch Connectors, "Southwest Microw Corp,".